

Femtosecond switching of strong light-matter interactions in microcavities with two-dimensional semiconductors

Armando Genco,^{1,*} Charalambos Louca,^{1,2,*} Cristina Cruciano,¹ Kok Wee Song,³ Chiara Trovatiello,^{1,4} Giuseppe Di Blasio,¹ Giacomo Sansone,⁵ Sam Randerson,⁶ Peter Claronino,⁶ Rahul Jayaprakash,⁶ Kenji Watanabe,⁷ Takashi Taniguchi,⁷ David G. Lidzey,⁶ Oleksandr Kyriienko,³ Stefano Dal Conte,¹ Alexander I. Tartakovskii,^{6,†} and Giulio Cerullo^{1,8,‡}

¹*Dipartimento di Fisica, Politecnico di Milano,
Piazza Leonardo Da Vinci 32, 20133 Milano, Italy*

²*NanoPhotonics Centre, Cavendish Laboratory,
Department of Physics, JJ Thompson Ave,
University of Cambridge, Cambridge, UK*

³*Department of Physics, University of Exeter, Stocker Road, EX4 4PY, Exeter, UK*

⁴*Department of Mechanical Engineering, Columbia University, New York, NY 10027, USA*

⁵*Dipartimento di Scienze Matematiche, Fisiche e Informatiche,
Università di Parma, Parco Area delle Scienze 7/A, 43124 Parma, Italy*

⁶*Department of Physics and Astronomy, University of Sheffield, Hounsfield Road, S3 7RH, Sheffield, UK*

⁷*Advanced Materials Laboratory, National Institute for
Materials Science, 1-1 Namiki, Tsukuba, 305-0044, Japan*

⁸*CNR-IFN, Piazza Leonardo da Vinci 32, Milano, 20133, Italy*

(Dated: August 2, 2024)

Ultrafast all-optical logic devices based on nonlinear light-matter interactions hold the promise to overcome the speed limitations of conventional electronic devices. Strong coupling of excitons and photons inside an optical resonator enhances such interactions and generates new polariton states which give access to unique nonlinear phenomena, such as Bose-Einstein condensation, used for all-optical ultrafast polariton transistors. However, the pulse energies required to pump such devices range from tens to hundreds of pJ, making them not competitive with electronic transistors. Here we introduce a new paradigm for all-optical switching based on the ultrafast transition from the strong to the weak coupling regime in microcavities embedding atomically thin transition metal dichalcogenides. Employing single and double stacks of hBN-encapsulated MoS₂ homobilayers with high optical nonlinearities and fast exciton relaxation times, we observe a collapse of the 55-meV polariton gap and its

revival in less than one picosecond, lowering the threshold for optical switching below 4 pJ per pulse, while retaining ultrahigh switching frequencies. As an additional degree of freedom, the switching can be triggered pumping either the *intra-* or the *interlayer* excitons of the bilayers at different wavelengths, speeding up the polariton dynamics, owing to unique interspecies excitonic interactions. Our approach will enable the development of compact ultrafast all-optical logical circuits and neural networks, showcasing a new platform for polaritonic information processing based on manipulating the light-matter coupling.

INTRODUCTION

All-optical switches based on nonlinear optical materials have been extensively investigated to overcome the speed limitations of electronic circuits, thanks to their potential to work at much higher frequencies owing to the inherently fast light-matter interactions underlying their operation [1]. Demonstrations of ultrafast all-optical logic gates have been achieved in a plethora of solid state platforms, exploiting optical nonlinearities ($\chi^{(2)}$ and $\chi^{(3)}$) [2, 3] and saturable absorption [4]. Notable examples employed microring resonators [5], plasmonic nanostructures [6], photonic crystals [7], metasurfaces [8], 2D materials [9] or even single molecules [10]. Such devices showcased switching times down to tens of femtoseconds, but usually at the expense of the switching energy or the *on/off* contrast [11, 12]. More recently, an optimal combination of femtosecond switching times and femtojoule operating energies has been obtained in an all-optical nonlinear device based on a lithium niobate waveguide [13], but with millimeter-scale lengths hindering the production of densely on-chip integrated circuits. Therefore, combining integration capabilities, full scalability and high performances in all-optical switches is still an open challenge.

Excitons in semiconducting materials embedded in optical resonators can be used for all-optical switching, as they show a highly nonlinear response when they are in strong coupling (SC) with resonant photons confined in the structure. In such a regime, the rate of coherent energy transfer between the energy-degenerate excitons and photons is higher than the loss rate, and new hybrid light-matter quasiparticles arise, called polaritons [14]. The energy splitting of the polariton states (Rabi splitting) is a direct measure of their coupling strength, which is proportional to the quality factor of the resonator and to the exciton absorption cross section.

Harnessing polaritonic nonlinear interactions is of key importance for a broad range of phenomena and applications, such as lasing [15], optical parametric amplification [16], Bose-Einstein con-

condensation (BEC) [17], or for quantum effects (polariton blockade) [18]. A combination of blueshift of the polariton states and gain in photoluminescence intensity occurring above the threshold of BEC has been used as operational principle of all-optical polariton logic devices and neural networks [19, 20]. Ultrafast optical switching (with switching times ≤ 1 ps) relying on BEC has been demonstrated even at room temperature [21–23], with the drawback of using high pulse energies to reach the condensation threshold (≈ 30 -300 pJ per pulse at least).

Alternative strategies for ultrafast all-optical switching in the SC regime rely on the modulation of the light-matter coupling strength acting on the exciton absorption, which produces a spectral shift of the polariton states, acting as a gate for the light transmitted/reflected by the device. Varying strongly the coupling strength would eventually lead to a complete transition from strong to weak coupling regime or viceversa [24]. SC can be switched off in strongly coupled optical microcavities comprising GaAs quantum wells through optical saturation of excitons [24, 25] or via electrically-tuned charge build-up [26]. Alternatively, it can be switched on by optically induced absorption, i.e. for inter sub-band transitions [27]. However, achieving complete *on/off* switching cycle below 1 ps acting on the coupling strength in these material platforms is not possible due to the long excitons and excited carriers lifetime [28].

Atomically thin transition metal dichalcogenides (TMDs) are promising nonlinear optical materials [29], where excitons remain stable up to room temperature due to large binding energies and oscillator strength [30, 31]. Owing to these properties, TMDs can easily enter the SC regime, when integrated in optical resonators [32, 33]. Recent studies of TMD polaritons aim to maximise nonlinear interactions going beyond the use of 1s neutral excitons, exploring higher Rydberg excitonic states, charged excitonic complexes, moiré or dipolar excitons [34–38]. Nonlinearities in MoS₂ bilayers have been shown to be particularly pronounced, due to a combination of Coulomb dipole-dipole interactions, phase space filling and interspecies interactions between hybridized intra- and interlayer excitons [39]. Moreover, the fast dynamics of TMD excitons [40] makes these materials very promising for ultrafast logic gates. While strong exciton nonlinear interactions can quench the Rabi splitting in TMD-based microcavities [41], all-optical ultrafast SC switching in atomically thin TMD systems has not been demonstrated.

Here we introduce a new strategy to perform all-optical switching in microcavities made of hBN-encapsulated MoS₂ bilayers, exploiting optical saturation of excitons and their fast relaxation times to produce an ultrafast collapse and revival of the SC regime. We employ femtosecond transient reflectivity (TR) spectroscopy to demonstrate sub-picosecond switching of the SC regime at pulse energies lower than 4 pJ, in ultra-compact devices comprising an atomically thin active material.

We show the full tuneability of this process through different degrees of freedom, such as pumping frequency, pulse power and bilayer configuration. The SC switching leads to a strong modulation of the polariton peaks splitting, reducing the initial energy separation from 42 meV to less than their linewidth, making them indistinguishable from a single peak. The Rabi splitting modulation is further enhanced by placing a stack of two bilayers separated by hBN in the cavity, going from 55 meV to a complete collapse, resulting in an effective extinction ratio of about 7.5 dB working in reflection. We further demonstrate an *on/off* SC switching frequency as high as 250 GHz, which can be extended up to 1 THz.

RESULTS

Static and dynamic optical behaviour of MoS₂ bilayers

The TMD structures used in our work are made of monolayers (MLs) and bilayers (BLs) of MoS₂ encapsulated in hBN, placed on distributed Bragg reflectors (DBRs), for the subsequent fabrication of optical microcavities. All the spectroscopy experiments in this work are performed at T = 8K. Figure 1a shows the Reflectance Contrast (RC) spectra of ML and BL MoS₂ outside the cavity. The absorption of the intralayer A exciton in the BL (X_{A-BL}) is higher than in the ML, due to presence of the additional layer. In the BL a new excitonic resonance appears at ≈ 2 eV, which is attributed to dipolar hybridized *interlayer* excitons (hIX) with a high oscillator strength, resulting from the coherent tunnelling of holes between the valence bands of the two layers (Fig. 1a inset) [42, 43].

We study the ultrafast response of MoS₂ excitons by ultrafast TR micro-spectroscopy. We deliver two collinear ≈ 100 -fs pulses, a narrow-band pump and a broad-band probe, focused on the sample using a microscope objective (Figure 1b). We then vary the delay time τ between them and monitor the changes in the broadband reflectivity spectrum of the probe (see Methods for experimental details). Figure 1c shows the differential reflectivity ($\Delta R/R$) map measured as a function of the probe photon energy and pump-probe delay for a BL MoS₂, tuning the energy of the pump pulses at ≈ 1.94 eV, in resonance with the X_{A-BL} .

Generally, the shape of the TR spectra in TMD MLs is a result of multiple effects, such as optical saturation (photo-bleaching), line broadening and spectral shift of the exciton peaks, leading to positive and negative TR signals around the exciton energies [44]. To show more clearly the temporal evolution of the exciton features in our system, we perform an analysis of the transient

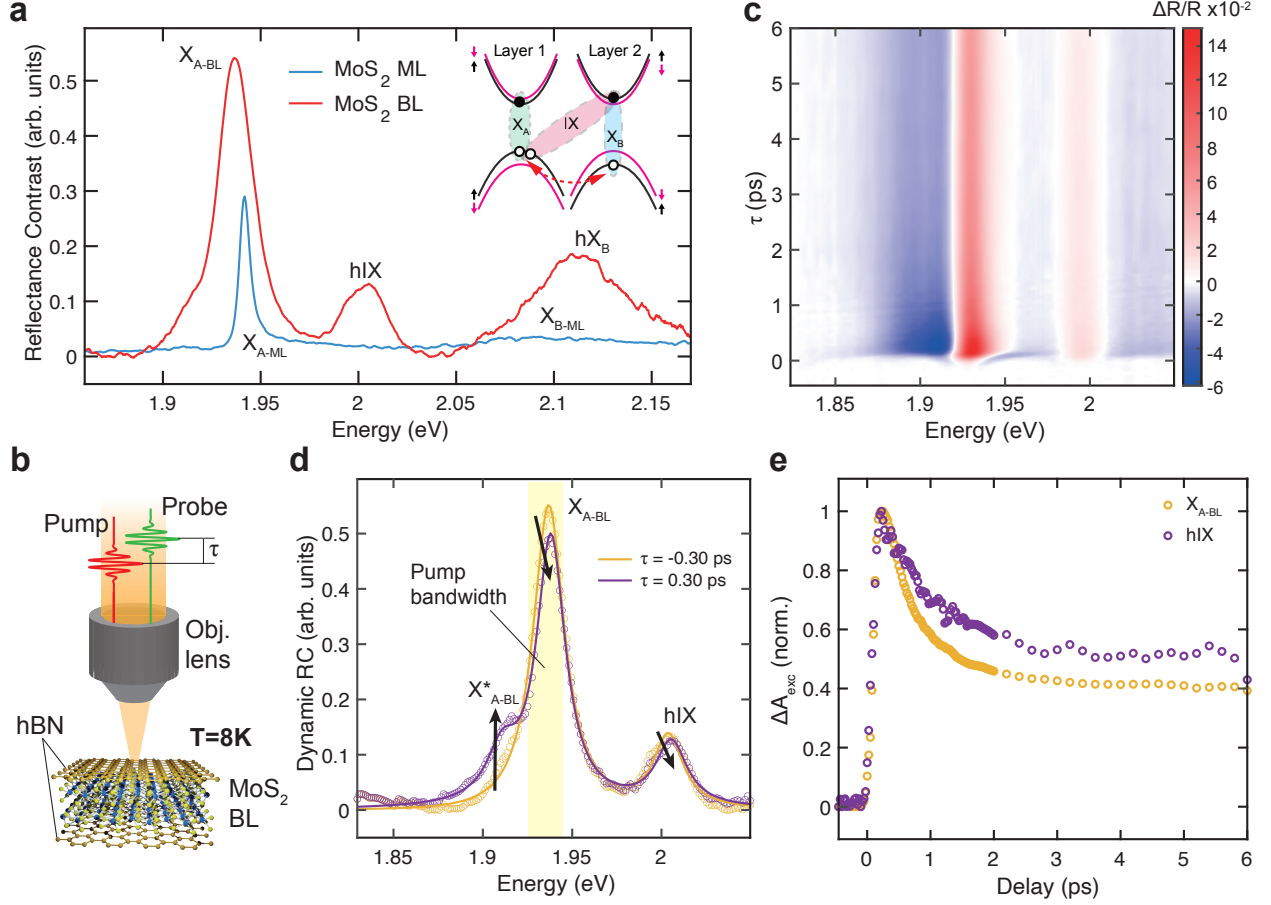


FIG. 1. **Optical characterization of the BL MoS₂** **a)** Static RC spectra of a ML and BL MoS₂ encapsulated in hBN. $RC = (R_{\text{sub}} - R_{\text{TMD}})/R_{\text{sub}}$, where R_{TMD} is the reflectance of the sample, while R_{sub} is taken on the substrate. Inset: sketch of the band diagram in MoS₂ BL; the dashed red line indicates the coherent tunnelling of holes. **b)** Sketch of the MoS₂ BL encapsulated in hBN (out of scale) measured by pump-probe micro-spectroscopy. **c)** Transient differential reflectivity map as a function of delay time τ and probe photon energy measured for MoS₂ BL. **d)** Dynamic RC of the MoS₂ BL at negative (before pulsed excitation) and positive (after pulsed excitation) delay times, extracted from the differential reflectivity map in **c)**. Solid curves show the Lorentzian fit of the dynamic RC. Black arrows show optical saturation and energy shift of the X_{A-BL} and hIX transitions, and the photo-induced absorption of the X_{A-BL}^{*} trion. The shaded yellow area displays the energy and bandwidth of the pump pulses. **e)** Normalized exciton peak amplitude variation (ΔA_{exc}) of X_{A-BL} and hIX, extracted from the dynamic RC at different time delays.

$\Delta R/R$ response based on the Transfer Matrix Method (TMM) to extract the time-dependent RC spectra of the material (see Methods for details) [45]. Figure 1d shows the MoS₂ BL dynamic RC spectrum at a delay of 0.3 ps (purple curve), compared to the one before the pump pulse (-0.3 ps, orange curve). We fit the dynamic RC with three Lorentzians (solid lines in Fig. 1d) to

extract the time-varying intensity and energy shift of each excitonic mode. After excitation, the X_{A-BL} peak is quenched and slightly blue-shifted, as a result of phase-space filling and Coulomb interactions occurring at high exciton densities [44, 46]. The small shoulder at 1.91 eV appearing at positive delays is instead related to a photo-induced absorption of the trion (X_{A-BL}^*) [47, 48]. Since the excitation pulses are in resonance with X_{A-BL} (shaded yellow area in Fig. 1d), at lower energies compared to hIX, we would expect negligible optical saturation of the latter if the two excitonic species were totally uncoupled. On the contrary, we observe a photo-bleaching of the hIX absorption, although less intense than in the X_{A-BL} case. This demonstrates their hybridization with intralayer excitons due to the coherent hole tunnelling between the valence bands of the two layers and to the fermionic interactions between holes of X_{A-BL} and hIX sharing the same valence band (see inset of Fig. 1a) [39].

Tracking the RC peak intensity as a function of the delay time, we can extract the ultrafast dynamics of the excitonic species (Fig. 1e). For both X_{A-BL} and hIX, the exciton population rises instantaneously (within the ≈ 100 fs temporal resolution of our setup), then decays exponentially, with about 50% of the initial population already relaxed within 2 ps (a comparison with MoS₂ ML exciton dynamics is reported in Supplementary Note S1). The simultaneous build-up of hIX population is again an indication of strong hybridization and fermionic interactions with intralayer excitons. The fast exciton decay time, resulting from both radiative and non-radiative relaxation processes of bright excitons [49, 50], the latter being significant in TMD bilayers, is also similar between X_{A-BL} and hIX.

Femtosecond switching of the strong coupling regime

We exploit the highly nonlinear exciton interactions in MoS₂ BL to drastically modify the light-matter coupling strength in microcavities on ultrafast time-scales. The microcavity samples are fabricated by covering the hBN-encapsulated MoS₂ heterostructures placed on DBRs with a transparent polymeric spacer (polymethylmethacrylate, PMMA) and a top silver (Ag) mirror, as illustrated in Fig. 2a. We perform k-space (Fourier) spectroscopy to image the angular dispersion of the monolithic cavity embedding the MoS₂ BL (Fig. 2b). Two distinct anticrossings appear when the cavity mode is in resonance with X_{A-BL} and hIX energies, a clear signature of the SC regime, resulting in upper, middle and lower polariton branches (UPB, MPB, LPB). Fitting the dispersion with a three coupled oscillators model, we extract Rabi splittings of $\Omega_{ABL} = 42$ meV and $\Omega_{hIX} = 23$ meV for X_{A-BL} and hIX respectively. The Rabi splitting for strongly coupled intralayer excitons in

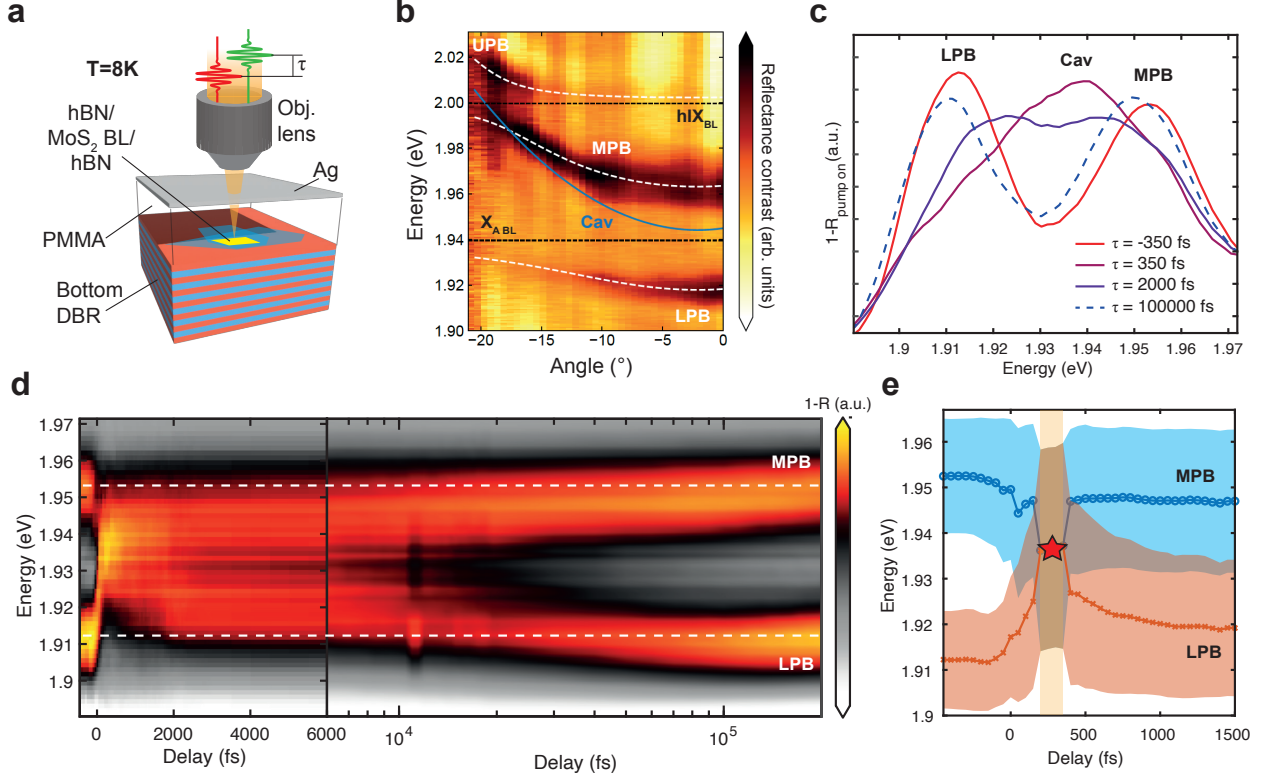


FIG. 2. **Ultrafast switching of strong coupling in a MoS₂ BL microcavity** **a)** Sketch of the MoS₂ BL microcavity structure measured by pump-probe spectro-microscopy. **b)** Color map of the angle-resolved RC spectra of a microcavity embedding a BL MoS₂ in strong coupling regime, showing two distinct anticrossings around the X_{A-BL} and hIX energies (black dashed lines) respectively. The coupled oscillators model fit (white dashed lines) and the cavity mode dispersion (blue line) are shown in overlay. **c)** 1-R spectra of the BL microcavity taken at different pump-probe delays, pumping the system at 1.94 eV with 3.75 pJ. Immediately after excitation, the polariton branches collapse in a central weakly coupled cavity mode. **d)** Color map of the 1-R spectra of the BL microcavity as a function of the pump-probe delay showing the ultrafast collapse and later revival of the MPB and LPB (white dashed lines). **e)** Results of Gaussian fits of the polariton/cavity modes dynamic spectra extracted from Fig. 2d. The blue (orange) trace refers to the MPB (LPB) peak energy, while the shaded areas depict the linewidth of the modes (Full Width Half Maximum, FWHM). Under the shaded yellow area only a weakly coupled cavity mode can be fitted, with the red star highlighting the crossing point between strong and weak coupling regimes.

a ML cavity is reduced to $\Omega_{AML} = 28$ meV, due to the lower oscillator strength (see Supplementary Note S2 for the coupled oscillators model fit of the ML cavity).

We use ultrafast TR spectroscopy to excite the MoS₂ BL-based microcavities with narrowband ultrashort pulses tuned at the energy of X_{A-BL} . To better visualize the dynamic behaviour of polariton spectrum, we plot directly the reflectance (1-R) spectra measured on the cavity as a

function of delay time and probe photon energy (Fig. 2c,d), while we include the TR data of the same measurement in Supplementary Note S3. Considering that in the spectral region of interest the reflectance of the cavity without the TMD is close to 1, plotting 1-R as a function of time is equivalent to showing the dynamic RC. We focus our analysis on incidence angles close to normal, on the anticrossing between the cavity mode and the X_{A-BL} , resulting in the MPB and LPB. In a stark contrast to the out-of-cavity experiments, we do not observe a strong quenching of the absorption, but rather measure huge shifts of the polariton states. At negative delays, MPB and LPB are clearly separated, located at 1.953 eV and 1.911 eV respectively. When the pump and probe pulses are synchronous, the two polariton peaks collapse symmetrically in one broad central peak at ≈ 1.94 eV (purple line in Fig. 2c). Already after 2 ps, the two polariton branches start to reappear, while after 100 ps they have almost completely recovered. The 1-R map as a function of the time delay (Fig. 2d) shows more clearly the complete collapse and revival of polaritons, which can be only explained as a reversible transition from the strong to the weak coupling regime. We note that this trend follows well the dynamic absorption of the excitonic species measured outside the cavity (Fig. 1e), being a direct consequence of density-dependent optical saturation of excitons.

We performed a quantitative analysis of the ultrafast behaviour of MoS₂ BL polaritons by fitting the experimental 1-R peaks with Gaussian functions. The results are shown in Fig. 2e, where the extracted peak energies and linewidths are plotted against the time delay up to 1.5 ps. Within few hundreds of femtoseconds from the zero-delay, the LPB shows a blueshift of about 27 meV, while the MPB redshifts by about 14 meV, merging in a single peak at about 250 fs. Such huge shifts cannot be explained just taking into account the bare exciton energy variations, which are in the order of only 5 meV (Fig. 1d). When the energy separation of the polariton states is lower than the linewidth of the cavity mode or the exciton, the anticrossing is not visible anymore and the system falls into the weak coupling regime (red star in Fig. 2e). Already after ≈ 500 fs, the SC is recovered. We note that in the weak coupling, the cavity mode is strongly broadened by the background absorption of the excitons, already broad due to excitation-induced dephasing [44]. Such broadening also affects the polariton peaks after the collapse, as shown in the color bars of Fig. 2e, which become more discernible only after 2 ps. We consider that the SC switching has been reached when the Rabi splitting is equal to the unperturbed exciton linewidth (the FWHM of X_{A-BL} is ≈ 20 meV in static conditions). On the other hand, considering as switching threshold the splitting being equal to the broader polariton linewidths would be a less stringent criterion. In the latter case the pump energy to induce a peak splitting collapse would be even lower, also resulting in a faster SC recovery.

We observed a similar SC collapse also in microcavities embedding a ML of MoS₂, but in that case the longer exciton lifetimes led to a much slower SC recovery, while the smaller Rabi splitting worsened the *on/off* contrast, i.e. the signal intensity ratio between the 1-R spectra of the cavity in the unperturbed SC and weak coupling conditions respectively (see Supplementary Note S4).

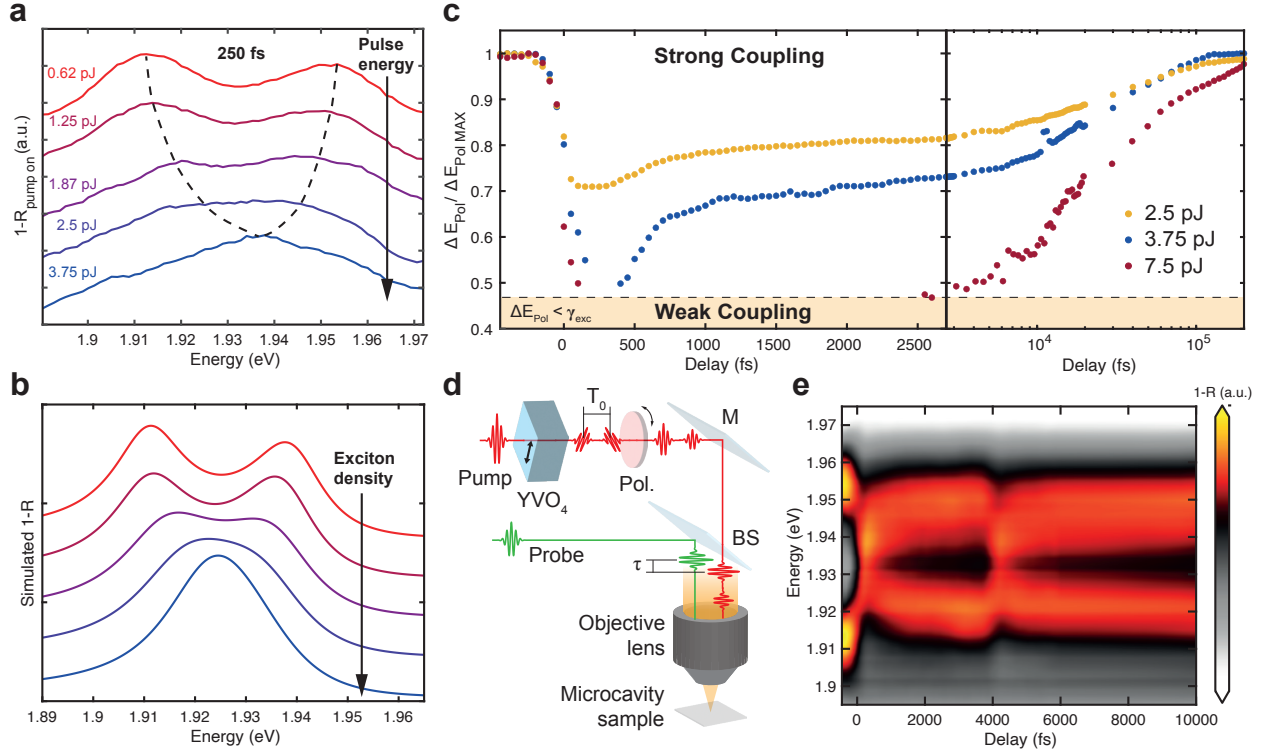


FIG. 3. Control of strong coupling switching **a)** BL cavity 1-R spectra taken at a delay time of 250 fs, pumping the system at increasingly higher pulse energies. **b)** Simulated cavity spectra for increasing exciton-polaritons densities in the MoS₂ BL. **c)** MPB-LPB energy difference as a function of delay time for ultrafast SC switching experiments in BL cavities at different pump pulse energies, normalized to the value before excitation. The weak coupling (yellow area) time window duration can be tuned by changing the excitation pulse energy. **d)** Sketch of the experimental configuration used to produce delayed double pump pulses. M: mirror; BS: beam splitter; Pol.: polarizer. **e)** Color map of the 1-R spectra of the BL microcavity as a function of the delay time, excited by double pump pulses delayed by ≈ 4 ps.

The pump pulse energy plays a major role in the SC switching dynamics, as shown in Fig. 3a where MoS₂ BL cavity spectra taken at a delay of 250 fs for different excitation pulse energies demonstrate the gradual quenching of the Rabi splitting. The SC collapse in TMD cavities is a direct consequence of exciton nonlinear interactions, which scale proportionally to their density [39]. We demonstrate this effect by carrying out theoretical simulations of the cavity 1-R spectra using the TMM (Fig. 3b), employing the MoS₂ BL optical constants calculated from the exciton

nonlinear absorption as a function of the density (see Supplementary Note S5). The match between experiments and simulations proves that the main cause behind the observed femtosecond switching of the SC regime is the optical saturation of MoS₂ BL excitons at high excitation densities, which recovers very rapidly due to the fast radiative and non-radiative exciton relaxation mechanisms in this system.

Figure 3c reports the MPB-LPB energy difference against the time delay, normalized with respect to its value before excitation. In this figure, the blue dots are related to the experiment reported in Fig. 2, performed at 3.75 pJ (pump fluence: 212 $\mu\text{J cm}^{-2}$), and show the recovery of SC occurring on two different time-scales, a fast one within 1 ps and a slow one which is concluded after ≈ 100 ps. We ascribe those two recovery steps to the population decay dynamics of the bare excitons (Fig. 1e). The dashed horizontal line represents the threshold for the weak coupling regime, when the polariton splitting is smaller than the exciton linewidth. Increasing or decreasing by few picojoules the excitation energy, we can extend the temporal window of weak coupling regime (7.5 pJ, red dots in Fig. 3c) or suppress completely the transition (2.5 pJ, yellow dots in Fig. 3c).

We provide a theoretical explanation on the energy dependent dynamic SC switching upon direct excitation of the intralayer excitons, considering several possible contributions to the dynamics. We note that the ≈ 1 ps timescale for the fast recovery coincides with the bare X_{A-BL} exciton fast decay. However, this short timescale cannot account for the later slower recovery (~ 100 ps) of the Rabi splitting, indicating that a significant exciton population remains in the sample and nonlinear phase space filling impacts the spectrum. One plausible explanation is the existence of long-lived dark excitonic states at lower energies [51, 52]. In this case photoexcited excitons can be transferred to such states which interact with light weakly, forming a reservoir that contributes to the nonlinear phase space filling. In a bilayer MoS₂, low-energy states are represented by spin-forbidden states due to spin-orbit coupling, or momentum-forbidden states [51] due to indirect bandgap [52]. These states possess a very long lifetime and can explain the TR dynamics. The corresponding model is summarized in the Methods, while we provide more details about the simulated polariton dynamics in Supplementary Note S6.

Leveraging on the ultrafast recovery times of SC in our samples, we demonstrate the possibility to modulate light-matter interactions at very high frequencies, illuminating the cavity with two subsequent pump pulses at 1.94 eV delayed by only ≈ 4 ps. To produce such pulse pair, we used a birefringent YVO₄ crystal with optical axis rotated by 45° with respect to the polarization of the incoming pump pulse, followed by a linear polarizer (see Fig. 3d and Methods for more details).

The first pulse energy was tuned to be slightly lower than the experiment in Fig. 2 in order to get a faster SC recovery, while the second pulse energy was adjusted to take into account the residual exciton population after the first pulse. The resulting transient 1-R map shows two reversible *on/off* cycles (Fig. 3e), proving a very fast switching frequency of ≈ 250 GHz. We note that this value was limited by technical constraints (the fixed delay between the pulse pair determined by the thickness of the available YVO₄ crystal), while the theoretical limit is given by the recovery time of the SC.

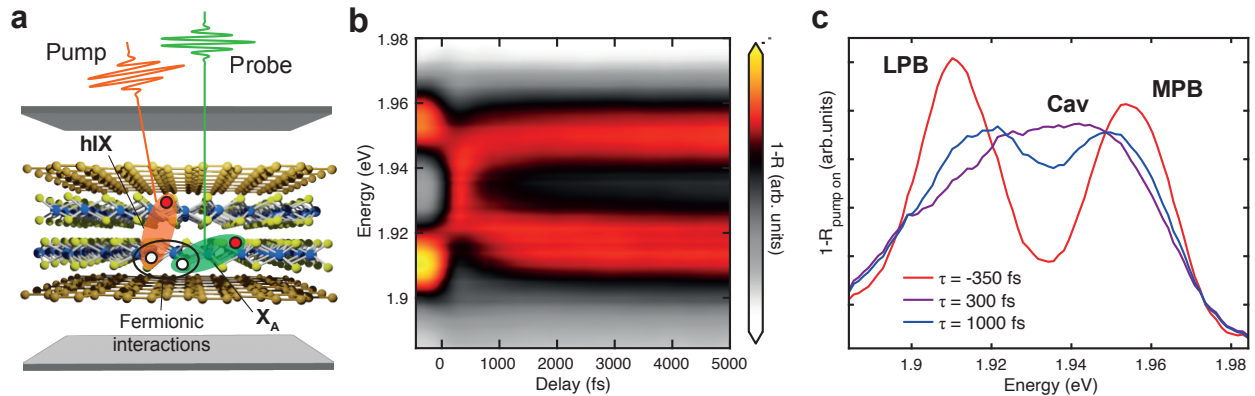


FIG. 4. **Ultrafast strong coupling switching by interspecies interactions.** **a)** Sketch of the MoS₂ BL cavity measured in pump-probe, exciting the hIX spectral region and probing the polariton states formed around X_{A- BL}. **b)** Color map of the 1-R spectra of the BL microcavity as a function of the delay time, exciting the hIX and probing the MPB-LPB spectral region. **c)** 1-R spectra of the BL microcavity pumping the hIX, taken at different pump-probe delay times. Already after 1 ps, the polariton peaks are clearly recovered.

Ultrafast SC switching by interspecies interactions

We exploit the interspecies exciton interactions specific of MoS₂ BL to generate optical saturation of X_{A- BL} acting on the hIX, exciting selectively the latter and probing the quenching of the Rabi splitting on X_{A- BL} (Fig. 4a). This process relies on nonlinear fermionic interactions (i.e. involving a single charge carrier constituting the exciton) between the two excitonic species: the X_{A- BL} valence band is shared with hIX, therefore exciting the latter causes optical quenching of the former, due to Pauli blocking of holes for X_{A- BL} [39]. Figure 4b shows the transient 1-R map of the MPB-LPB, pumping the hIX of the BL: the femtosecond switching of SC regime occurs very clearly also in this case. Comparing this result with the previous case of resonant X_{A- BL} pumping (Fig. 2c), the fast SC recovery is even more distinct, with the two polariton peaks being clearly

visible and well separated already after 1 ps, as shown in Figure 4c.

The dynamics of the nonlinear response when pumping in resonance with the hIX is also consistent with the developed model based on the nonlinear saturation and phase space filling from the long-lived states (see Methods). In this case, we considered similar lifetimes for hIX compared to X_{A-BL} , but we assumed the rate for transferring the pumped hIX to the long-lived reservoir states contributing to the phase space filling to be smaller than in the X_{A-BL} case. This may be understood as the result of the hIX's wavefunction spreading in the out-of-plane direction. This implies that hIX is less 2D than X_{A-BL} , leading to a weaker scattering effect with disorder and to a smaller transfer rate. Furthermore, thermalization through exciton-phonon scattering is another important mechanism converting the bright states into momentum-dark states which may also gives smaller transfer rate upon hIX pumping. These scattering effects yield a faster recovery of SC, in agreement with our experimental observation (see Supplementary Note S6).

Another effect leading to faster recovery in the hIX pumping scheme is the mitigation of the Pauli blockade. In contrast to X_{A-BL} pumping, the pumped exciton only shares holes with the probed exciton but not the electrons [39], see Fig. 4a, leading to a weaker saturation effect. This can also result in a faster recovery of SC if similar conditions as in X_{A-BL} case are used (except the pump photon energy). Combining the effects of a smaller bright-to-dark exciton transfer rate and weaker Pauli blockade, the influence of the reservoir long-lived states is less significant exciting the hIX. Therefore, a faster recovery time of SC is easier to achieve in this case. Such fast recovery would allow to further increase the switching frequency, up to ≈ 1 THz. We underline that to achieve such hIX-induced Rabi quenching we use an excitation energy of 4.37 pJ, only moderately higher compared to the resonant excitation case. Higher pulse energies will increase the recovery time and the weak coupling time window.

SC switching in a double BL microcavity

Finally, we fabricated a device comprising two vertically stacked bilayer MoS_2 separated by an hBN spacer of 40 nm. We placed this structure in a microcavity made of the same DBR and silver mirror used in the single BL cavity, with a PMMA spacer between the TMD stack and the top mirror (Fig. 5a). Similarly to microcavities with multiple quantum wells [53], the SC is enhanced in this sample, as the Rabi splitting is increased to 55 meV due to the additional BL unit (see Supplementary Note S7 for the coupled oscillators model fit of the strongly coupled cavity dispersion). Figure 5b shows a comparison between the static 1-R spectra of a single BL (blue line)

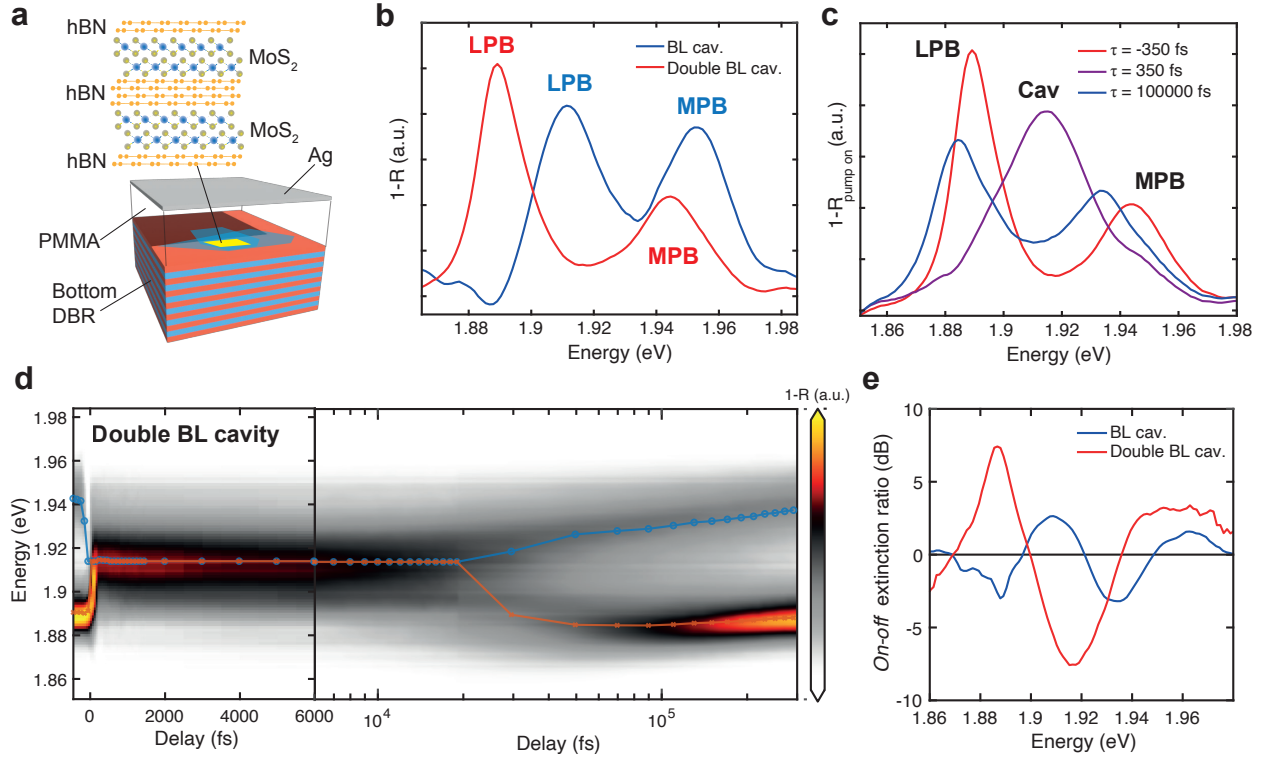


FIG. 5. **Ultrafast switching of a double BL microcavity.** **a)** Sketch of the microcavity embedding a double BL of MoS₂. **b)** Static 1-R spectra of the single BL compared to the double BL microcavity, showing a redshift of the MPB-LPB and an increased polariton splitting in the latter. **c)** 1-R spectra of the double BL microcavity excited with pump pulses at 1.91 eV and 8.25 pJ, taken at different pump-probe delays. **d)** Color map of the 1-R spectra of the double BL microcavity versus pump-probe delay showing the ultrafast collapse and later revival of the SC. The orange (blue) line in overlay displays the fitted peak energy of the LPB (MPB) or the weakly coupled cavity mode. **e)** Effective *on/off* extinction ratio calculated from the 1-R spectra taken at -350 fs and 350 fs, for the single (blue line) and double BL cavity (red line).

and a double BL (red line) cavity, taken at small angles. It clearly appears that the MPB-LPB peaks are more separated in the double BL cavity compared to the single BL sample, being also redshifted, as an effect of the more negative detuning of the former. The negative detuning also leads to a decrease of the LPB linewidth in the double BL cavity, being more cavity-like.

By exciting the double BL cavity with pump pulses resonant with X_{A-BL} , we observed again an ultrafast collapse of the MPB-LPB polariton peaks into a weakly coupled cavity mode, followed by their later recovery (Fig. 5c). We note that the pulse energy used for this experiment (8.25 pJ) was not adjusted to obtain a sub-ps SC recovery, but just to demonstrate the SC switching. Figure 5d shows the full dynamics of the SC collapse and recovery in the double BL cavity, where the energy separation between MPB and LPB (blue and red lines respectively) drops from ≈ 55 meV

to zero immediately after the pump pulse. Considering the unperturbed SC condition as the *on* state of the optical switch and the weak coupling as the *off* state, we calculated the spectral power extinction ratio (ER) from the $1 - R$ spectra before and after the pump pulse, taken at -350 fs and 350 fs respectively, where $\text{ER}(\text{dB}) = 10 \log((1 - R_{\text{on}})/(1 - R_{\text{off}}))$. The ER is increased significantly in the double BL cavity compared to the single BL device, over a broad energy range, as shown in Fig. 5e. For both the devices, the maximum ER in absolute value is reached around the energy of the weakly coupled cavity mode, between the LPB and MPB, which transmits (reflects) more during the *off* (*on*) state. While for the single BL the ER absolute value reaches 3.2 dB at 1.932 eV, it is enhanced up to 7.5 dB at 1.915 eV in the double BL. It is worth to mention that the ER is also high in the spectral regions of the LPB and MPB, where it shows opposite sign, meaning that the optical switch can be used in direct or reverse mode just by changing the operational wavelength. We note that working at high frequencies the effective extinction ratio for a second switching event decreases due to the residual exciton population after the first pulse excitation (e.g. by about four times in the double pump pulse experiment shown in Fig. 3). We foresee that this drawback can be mitigated by reducing the long exciton decay component, for example suppressing the exciton scattering to dark states and using a different optical resonator with higher quality factor and smaller mode volume, to induce a strong Purcell effect.

DISCUSSION

In summary, we exploit the transient behaviour of MoS₂ exciton-polaritons to demonstrate ultra-fast optical switches, whose operational principle is based on the instantaneous transition from the strong to the weak coupling regime due to optical saturation of excitons, which can recover on the sub-picosecond timescale. The MoS₂ BL system uniquely combines nanometric thickness, large nonlinearities and large Rabi splitting with short lifetimes, with the latter enabling observation of the exceptionally fast recovery. Furthermore, we show that by increasing slightly the pump pulse energies above the threshold for the SC collapse, the weak coupling time window can be significantly extended and deterministically controlled, being sensitive to energy variations of hundreds of femtojoules and below, crucially important for sensing and low light applications [54]. This system, also, offers additional degrees of freedom. It can operate at different excitation energies, for example in resonance with either intra- or interlayer excitons, leveraging on the strong interspecies interactions between these excitonic species, unique to the MoS₂ BLs. We foresee this property to be particularly useful for multiplexed logic operations [55]. Owing to the fast recovery of SC, we

were able to perform subsequent switching events delayed by 4 ps, demonstrating an operational frequency of ≈ 250 GHz. Considering the sub-ps SC switching time, this frequency can be pushed up to 1 THz, surpassing even the fastest electronic transistors demonstrated so far [56]. We also demonstrate that using a microcavity with two stacked MoS₂ BLs can boost the Rabi splitting and greatly enhance the *on/off* extinction ratio, reaching a maximum of 7.5 dB in a single switching event. An improvement of the optical resonator quality factor and a shorter exciton lifetime will lead to even greater *on/off* contrast for high frequency switching.

Our work highlights atomically thin TMDs as a flexible system with rich physics in which sub-ps all-optical switching can be achieved and finely controlled. The insights provided can be pivotal for the development of TMD-based high speed all-optical circuits. Moreover, the developed ultrafast nonlinear switching unit can improve the performance of optical neural networks [57, 58] acting as an all-optical nonlinear activation function. We believe that further progress in boosting the nonlinear interactions of TMD excitons, for example employing localized excitons in moiré heterostructures, could reduce even more the energy required for the ultrafast switching processes, reaching eventually the quantum regime of operation down to a few photons, eventually leading to single-photon transistor-type devices [59, 60]. The ultrafast switching operation can be extended in principle up to room temperature using our devices, owing to the large binding energies of TMD excitons. Considering also the nanometric thickness of each hBN/BL/hBN stack, a microcavity could be filled by many TMD units, greatly increasing the Rabi splitting and subsequently the spectral shifts when used as ultrafast switches, which will lead to enhanced *on/off* extinction ratio. Moreover, the integration of electrical contacts in the microcavity structures [61] would enable the fabrication of electro-optical interfaces by tuning the electrostatic doping and electric field, which can provide giant shifts of the hIX energy in MoS₂ BLs [43], also enhancing their nonlinear interactions. Finally, highly nonlinear TMD systems combined with novel light-confining nanostructures supporting photonic resonances of high quality factor, such as quasi-bound states in the continuum [62, 63], will allow the development of ultra-compact nanodevices, easy to be integrated in planar photonic circuits architectures.

Developing ultrafast all-optical switches based on the transition from the strong to the weak coupling regime would be crucial also to unveil more exotic physical phenomena. The crossing point between the strong and weak coupling regimes, called exceptional point, enfolds exotic physics arising from the non-Hermitian Hamiltonian describing such condition [64]. Both the Hamiltonian eigenvalues and their corresponding eigenstates collapse in exceptional points, which for systems of coupled exciton and photon states translates in their energy and losses becoming identical, making

the system very sensitive to external perturbations. Changing non-adiabatically the parameters of the coupled system in order to encircle the exceptional point can produce topological effects and chiral mode conversions, where the direction of the encirclement dictates the final state of the system [65]. Owing to the ultrafast collapse and recovery of SC, our system could be used to demonstrate for the first time this effect in planar microcavities.

METHODS

Sample Fabrication

The hBN/MoS₂/hBN heterostructures were assembled using a polydimethylsiloxane (PDMS) polymer stamp method. The PMMA spacer for the monolithic cavity was deposited using a spin-coating technique, while a silver mirror of 45 nm thickness was thermally evaporated on top of it.

Optical Measurements

For the transient reflectivity measurements 100-fs pulses from an amplified Ti:Sapphire laser at 2 kHz repetition rate are used. The laser output is split in two beams. A portion of the laser output is utilized to drive a non-collinear optical parametric amplifier (NOPA), which allows tuning the pump wavelength. The rest is used for the generation of the broadband white light probe pulse by focusing the beam on a sapphire plate. The delay between pump and probe pulses is controlled by a mechanical delay line. The pulses are combined collinearly and focused on the sample using a 50x objective, resulting in a spot size of $\approx 1.5 \mu\text{m}$. The sample is kept in a helium cryostat at 8 K. The differential reflectivity ($\Delta R/R$) spectra are recorded at various time delays τ to track the changes induced by the pump. Specifically, the reflectivity spectrum of the probe with the pump on, R_{PumpOn} , is compared at each delay with a reference spectrum obtained when the pump is off, R_{PumpOff} . These are used to calculate $\frac{\Delta R}{R} = \frac{R_{\text{PumpOn}} - R_{\text{PumpOff}}}{R_{\text{PumpOff}}}$, shown in the TR maps. The dynamic probe maps are extracted from a combination of the measured RC spectrum with the pump off and the $\Delta R/R$ maps, as $R_{\text{PumpOn}} = R_{\text{PumpOff}}(1 + \frac{\Delta R}{R})$. For the double pump pulses experiments, we use a thick YVO₄ birefringent crystal with optical axis rotated at 45° with respect to the vertical pump polarization, which produces a replica of the pulse with horizontal polarization delayed by ≈ 4 ps. The rotation of a subsequent polarizer is changed to finely adjust the energy of each pulse in order to ensure the SC recovery after each excitation pulse.

Transfer Matrix Method Analysis

In order to extract the spectral and temporal evolution of the excitonic optical properties from the $\Delta R/R$ maps, we follow a procedure recently reported in refs [45, 66]. The transient reflectivity $R(\omega, \tau)$ of MoS₂ BL at each delay time is determined from the equilibrium reflectivity $R(\omega)$, which is reconstructed from the TMM fit of the static RC spectrum, and the transient reflectivity $\frac{\Delta R}{R}(\omega, \tau)$, following this relation:

$$R(\omega, \tau) = R(\omega) \left(\frac{\Delta R}{R}(\omega, \tau) + 1 \right)$$

Then, the dynamic RC is obtained by applying the formula: $\text{RC}(\omega, \tau) = 1 - (R(\omega, \tau)/R_{\text{sub}})$, where the substrate reflectivity R_{sub} is simulated with the TMM. See Supplementary Note S5 for more details on the TMM simulations.

Theoretical Model for the Polariton Dynamics

To gain further insight into the dynamics in the system, we develop a mean-field model that captures the main trends in our experiment over different excitation regimes. The Hamiltonian corresponds to the coupled cavity-photon system, where the $X_{\text{A-BL}}$ mode (being the probed A exciton of a homobilayer) hybridizes with the cavity mode. The Hamiltonian reads

$$H = \begin{bmatrix} E_c + i\kappa & \frac{1}{2}g(n_X)\Omega_{\text{ABL}} \\ \frac{1}{2}g(n_X)\Omega_{\text{ABL}} & E_{\text{ABL}} + i\gamma \end{bmatrix},$$

where E_c and κ are the energy and linewidth of the cavity photon, and E_{ABL} and γ are the energy and linewidth of the probed exciton. In the Hamiltonian above Ω_{ABL} is the Rabi splitting at weak pumping, and $g(n_X) = e^{-\alpha n_X}$ is the dimensionless nonlinear coupling, with α being the nonlinear phase space filling (saturation) coefficient [67]. The magnitude of the Rabi splitting is dependent on the total number of excitons in the system, n_X . In general $n_X(t) = n_p(t) + n_R(t)$ is time-dependent, and includes excitons (electron-hole pairs) from different states. Specifically, we separate the two fractions corresponding to n_p and n_R being the population of the pumped exciton and the long-lived excitons in the reservoir. Crucially, both contribute to the nonlinear saturation effect. The dynamics of excitonic fractions can be described by rate equations defining the transfer and population redistribution, which read

$$\begin{aligned} \frac{dn_p}{dt} &= -\gamma_p n_p - r n_p + \Theta(t), \\ \frac{dn_R}{dt} &= -\gamma_R n_R + r n_p, \end{aligned}$$

where γ_p is the pumped exciton decay rate, γ_R is the decay rate of the long-lived exciton in the reservoir, and r is the rate constant for transferring the pumped excitons into the reservoir. The function $\Theta(t)$ depends on the pump laser profile in time. For example, $\Theta(t)$ can be a Heaviside step function to model the pump as an on-off switching field. In this model, we assume $\gamma_R \approx \gamma_p/100$ for the long-lived states corresponding to 100 ps decay time, and consider the decay timescale being similar to that of spin-forbidden dark states [68]. In fact, the decay time may be different, but this does not change our later conclusion in a qualitative way. Furthermore, when considering a spin-conserving process, we let the transfer rate be comparable to the pumped exciton decay rate [69], $r \approx \gamma_p$, such that this allows the pumped exciton transfer into the reservoir. With this, we find a good qualitative agreement between the theoretical spectrum and the experimental measurement (see Supplementary Note S6). Particularly, the theory demonstrated the excitation pulse energy dependence of the recovery time of SC.

ACKNOWLEDGEMENTS

AG and GC acknowledge support by the European Union Marie Skłodowska-Curie Actions project ENOSIS H2020-MSCA-IF-2020-101029644. CT acknowledges the European Union’s Horizon Europe research and innovation programme under the Marie Skłodowska-Curie PIONEER HORIZON-MSCA-2021-PF-GF grant agreement No 101066108. AG, CT, SDC and GC acknowledge funding from the European Horizon EIC Pathfinder Open programme under grant agreement no. 101130384 (QUONDENSATE). This work reflects only authors’ view and the European Commission is not responsible for any use that may be made of the information it contains. AIT and SR acknowledge financial support of the EPSRC grants EP/V006975/1, EP/V026496/1 and EP/S030751/1. OK and KWS acknowledge the support from UK EPSRC grant EP/X017222/1.

The authors declare no competing interests.

AUTHOR CONTRIBUTIONS

AG, CL, CC and CT carried out the optical spectroscopy experiments with contribution from GDB and GS. CL and SR fabricated the 2D samples. KW and TT synthesized the high quality hBN. PC, RJ and DGL fabricated the microcavities. AG, CL, CC, GDB and GS analyzed the data with contribution from SDC, AIT and GC. AG performed the transfer matrix simulations.

KWS and OK developed the theory on dynamic optical saturation in microcavities. AG, CL and GC wrote the manuscript with contribution from all other co-authors. DGL, OK, SDC, AIT and GC managed various aspects of the project. SDC, AIT and GC supervised the project.

DATA AVAILABILITY

The data that support the findings of this study are available from the corresponding authors upon reasonable request.

CODE AVAILABILITY

The computer codes and algorithms used to process the data included in this study are available from the corresponding authors upon reasonable request.

INCLUSION AND ETHICS STATEMENT

All collaborators of this study that have fulfilled the criteria for authorship required by Nature Portfolio journals have been included as authors, as their participation was essential for the design and implementation of the study. Roles and responsibilities were agreed among collaborators ahead of the research. This work includes findings that are locally relevant, which have been determined in collaboration with local partners. This research was not severely restricted or prohibited in the setting of the researchers, and does not result in stigmatization, incrimination, discrimination or personal risk to participants. Local and regional research relevant to our study was taken into account in citations.

ADDITIONAL INFORMATION

Supplementary Information is available for this paper.

* Contributed equally

† a.tartakovskii@sheffield.ac.uk

‡ giulio.cerullo@polimi.it

[1] D. A. Miller, Are optical transistors the logical next step?, *Nature Photonics* **4**, 3 (2010).

- [2] G. Grinblat, M. P. Nielsen, P. Dichtl, Y. Li, R. F. Oulton, and S. A. Maier, Ultrafast sub-30-fs all-optical switching based on gallium phosphide, *Science advances* **5**, eaaw3262 (2019).
- [3] G. Assanto, G. Stegeman, M. Sheik-Bahae, and E. Van Stryland, All-optical switching devices based on large nonlinear phase shifts from second harmonic generation, *Applied Physics Letters* **62**, 1323 (1993).
- [4] N. Iizuka, K. Kaneko, and N. Suzuki, All-optical switch utilizing intersubband transition in gan quantum wells, *IEEE journal of quantum electronics* **42**, 765 (2006).
- [5] V. R. Almeida, C. A. Barrios, R. R. Panepucci, and M. Lipson, All-optical control of light on a silicon chip, *Nature* **431**, 1081 (2004).
- [6] Y. Fu, X. Hu, C. Lu, S. Yue, H. Yang, and Q. Gong, All-optical logic gates based on nanoscale plasmonic slot waveguides, *Nano letters* **12**, 5784 (2012).
- [7] K. Nozaki, T. Tanabe, A. Shinya, S. Matsuo, T. Sato, H. Taniyama, and M. Notomi, Sub-femtojoule all-optical switching using a photonic-crystal nanocavity, *Nature Photonics* **4**, 477 (2010).
- [8] S. A. Mann, N. Nookala, S. C. Johnson, M. Cotrufo, A. Mekawy, J. F. Klem, I. Brener, M. B. Raschke, A. Alù, and M. A. Belkin, Ultrafast optical switching and power limiting in intersubband polaritonic metasurfaces, *Optica* **8**, 606 (2021).
- [9] M. Ono, M. Hata, M. Tsunekawa, K. Nozaki, H. Sumikura, H. Chiba, and M. Notomi, Ultrafast and energy-efficient all-optical switching with graphene-loaded deep-subwavelength plasmonic waveguides, *Nature Photonics* **14**, 37 (2020).
- [10] J. Hwang, M. Pototschnig, R. Lettow, G. Zumofen, A. Renn, S. Götzinger, and V. Sandoghdar, A single-molecule optical transistor, *Nature* **460**, 76 (2009).
- [11] H. Qi, X. Wang, X. Hu, Z. Du, J. Yang, Z. Yu, S. Ding, S. Chu, and Q. Gong, All-optical switch based on novel physics effects, *Journal of Applied Physics* **129** (2021).
- [12] Z. Chai, X. Hu, F. Wang, X. Niu, J. Xie, and Q. Gong, Ultrafast all-optical switching, *Advanced Optical Materials* **5**, 1600665 (2017).
- [13] Q. Guo, R. Sekine, L. Ledezma, R. Nehra, D. J. Dean, A. Roy, R. M. Gray, S. Jahani, and A. Marandi, Femtojoule femtosecond all-optical switching in lithium niobate nanophotonics, *Nature Photonics* **16**, 625 (2022).
- [14] A. V. Kavokin, J. J. Baumberg, G. Malpuech, and F. P. Laussy, *Microcavities*, Vol. 21 (Oxford university press, 2017).
- [15] S. Kéna-Cohen and S. Forrest, Room-temperature polariton lasing in an organic single-crystal microcavity, *Nature Photonics* **4**, 371 (2010).
- [16] M. Saba, C. Ciuti, J. Bloch, V. Thierry-Mieg, R. André, L. S. Dang, S. Kundermann, A. Mura, G. Bongiovanni, J. Staehli, *et al.*, High-temperature ultrafast polariton parametric amplification in semiconductor microcavities, *Nature* **414**, 731 (2001).
- [17] H. Deng, H. Haug, and Y. Yamamoto, Exciton-polariton bose-einstein condensation, *Reviews of modern physics* **82**, 1489 (2010).

- [18] A. Delteil, T. Fink, A. Schade, S. Höfling, C. Schneider, and A. İmamoğlu, Towards polariton blockade of confined exciton–polaritons, *Nature materials* **18**, 219 (2019).
- [19] D. Ballarini, M. De Giorgi, E. Cancellieri, R. Houdré, E. Giacobino, R. Cingolani, A. Bramati, G. Gigli, and D. Sanvitto, All-optical polariton transistor, *Nature communications* **4**, 1778 (2013).
- [20] D. Ballarini, A. Gianfrate, R. Panico, A. Opala, S. Ghosh, L. Dominici, V. Ardizzone, M. De Giorgi, G. Lerario, G. Gigli, et al., Polaritonic neuromorphic computing outperforms linear classifiers, *Nano Letters* **20**, 3506 (2020).
- [21] J. Feng, J. Wang, A. Fieramosca, R. Bao, J. Zhao, R. Su, Y. Peng, T. C. Liew, D. Sanvitto, and Q. Xiong, All-optical switching based on interacting exciton polaritons in self-assembled perovskite microwires, *Science Advances* **7**, eabj6627 (2021).
- [22] F. Chen, H. Li, H. Zhou, S. Luo, Z. Sun, Z. Ye, F. Sun, J. Wang, Y. Zheng, X. Chen, et al., Optically controlled femtosecond polariton switch at room temperature, *Physical Review Letters* **129**, 057402 (2022).
- [23] A. V. Zasedatelev, A. V. Baranikov, D. Urbonas, F. Scafirimuto, U. Scherf, T. Stöferle, R. F. Mahrt, and P. G. Lagoudakis, A room-temperature organic polariton transistor, *Nature Photonics* **13**, 378 (2019).
- [24] R. Butté, G. Delalleau, A. Tartakovskii, M. Skolnick, V. Astratov, J. Baumberg, G. Malpuech, A. Di Carlo, A. Kavokin, and J. Roberts, Transition from strong to weak coupling and the onset of lasing in semiconductor microcavities, *Physical Review B* **65**, 205310 (2002).
- [25] N. Takemura, M. D. Anderson, S. Trebaol, S. Biswas, D. Oberli, M. T. Portella-Oberli, and B. Deveaud, Dephasing effects on coherent exciton-polaritons and the breakdown of the strong coupling regime, *Physical Review B* **92**, 235305 (2015).
- [26] P. Tsotsis, S. I. Tsintzos, G. Christmann, P. G. Lagoudakis, O. Kyriienko, I. A. Shelykh, J. J. Baumberg, A. V. Kavokin, Z. Hatzopoulos, P. S. Eldridge, and P. G. Savvidis, Tuning the energy of a polariton condensate via bias-controlled rabi splitting, *Phys. Rev. Appl.* **2**, 014002 (2014).
- [27] G. Günter, A. A. Anappara, J. Hees, A. Sell, G. Biasiol, L. Sorba, S. De Liberato, C. Ciuti, A. Tredicucci, A. Leitenstorfer, et al., Sub-cycle switch-on of ultrastrong light–matter interaction, *Nature* **458**, 178 (2009).
- [28] B. Sermage, B. Deveaud, K. Satzke, F. Clerot, C. Dumas, N. Roy, D. Katzer, F. Mollot, R. Planel, M. Berz, et al., Radiative recombination of free excitons in gaas quantum wells, Superlattices and microstructures **13**, 271 (1993).
- [29] X. Wen, Z. Gong, and D. Li, Nonlinear optics of two-dimensional transition metal dichalcogenides, *InfoMat* **1**, 317 (2019).
- [30] G. Wang, A. Chernikov, M. M. Glazov, T. F. Heinz, X. Marie, T. Amand, and B. Urbaszek, Colloquium: Excitons in atomically thin transition metal dichalcogenides, *Reviews of Modern Physics* **90**, 021001 (2018).

- [31] K. Novoselov, A. Mishchenko, A. Carvalho, and A. Castro Neto, 2d materials and van der waals heterostructures, *Science* **353**, aac9439 (2016).
- [32] C. Schneider, M. M. Glazov, T. Korn, S. Höfling, and B. Urbaszek, Two-dimensional semiconductors in the regime of strong light-matter coupling, *Nature communications* **9**, 2695 (2018).
- [33] H. Kang, J. Ma, J. Li, X. Zhang, and X. Liu, Exciton polaritons in emergent two-dimensional semiconductors, *ACS nano* **17**, 24449 (2023).
- [34] J. Gu, V. Walther, L. Waldecker, D. Rhodes, A. Raja, J. C. Hone, T. F. Heinz, S. Kéna-Cohen, T. Pohl, and V. M. Menon, Enhanced nonlinear interaction of polaritons via excitonic rydberg states in monolayer wse2, *Nature communications* **12**, 2269 (2021).
- [35] R. Emmanuele, M. Sich, O. Kyriienko, V. Shahnazaryan, F. Withers, A. Catanzaro, P. Walker, F. Benimetskiy, M. Skolnick, A. Tartakovskii, *et al.*, Highly nonlinear trion-polaritons in a monolayer semiconductor, *Nature communications* **11**, 3589 (2020).
- [36] T. Lyons, D. Gillard, C. Leblanc, J. Puebla, D. Solnyshkov, L. Klompmaker, I. Akimov, C. Louca, P. Muduli, A. Genco, *et al.*, Giant effective zeeman splitting in a monolayer semiconductor realized by spin-selective strong light-matter coupling, *Nature Photonics* **16**, 632 (2022).
- [37] L. Zhang, F. Wu, S. Hou, Z. Zhang, Y.-H. Chou, K. Watanabe, T. Taniguchi, S. R. Forrest, and H. Deng, Van der waals heterostructure polaritons with moiré-induced nonlinearity, *Nature* **591**, 61 (2021).
- [38] B. Datta, M. Khatoniar, P. Deshmukh, F. Thouin, R. Bushati, S. De Liberato, S. K. Cohen, and V. M. Menon, Highly nonlinear dipolar exciton-polaritons in bilayer mos2, *Nature communications* **13**, 6341 (2022).
- [39] C. Louca, A. Genco, S. Chiavazzo, T. P. Lyons, S. Randerson, C. Trovatiello, P. Claronino, R. Jayaprakash, X. Hu, J. Howarth, *et al.*, Interspecies exciton interactions lead to enhanced nonlinearity of dipolar excitons and polaritons in mos2 homobilayers, *Nature Communications* **14**, 3818 (2023).
- [40] G. Moody, J. Schaibley, and X. Xu, Exciton dynamics in monolayer transition metal dichalcogenides, *JOSA B* **33**, C39 (2016).
- [41] J. Zhao, A. Fieramosca, K. Dini, R. Bao, W. Du, R. Su, Y. Luo, W. Zhao, D. Sanvitto, T. C. Liew, *et al.*, Exciton polariton interactions in van der waals superlattices at room temperature, *Nature Communications* **14**, 1512 (2023).
- [42] I. C. Gerber, E. Courtade, S. Shree, C. Robert, T. Taniguchi, K. Watanabe, A. Balocchi, P. Renucci, D. Lagarde, X. Marie, and B. Urbaszek, Interlayer excitons in bilayer MoS₂ with strong oscillator strength up to room temperature, *Physical Review B* **99**, 1 (2019).
- [43] N. Leisgang, S. Shree, I. Paradisanos, L. Sponfeldner, C. Robert, D. Lagarde, A. Balocchi, K. Watanabe, T. Taniguchi, X. Marie, *et al.*, Giant Stark splitting of an exciton in bilayer MoS₂, *Nature Nanotechnology* **15**, 901 (2020).

- [44] F. Katsch, M. Selig, and A. Knorr, Exciton-scattering-induced dephasing in two-dimensional semiconductors, *Physical Review Letters* **124**, 257402 (2020).
- [45] C. Trovatiello, F. Katsch, Q. Li, X. Zhu, A. Knorr, G. Cerullo, and S. Dal Conte, Disentangling many-body effects in the coherent optical response of 2d semiconductors, *Nano Letters* **22**, 5322 (2022).
- [46] V. Shahnazaryan, I. Iorsh, I. A. Shelykh, and O. Kyriienko, Exciton-exciton interaction in transition-metal dichalcogenide monolayers, *Phys. Rev. B* **96**, 115409 (2017).
- [47] A. Genco, C. Trovatiello, C. Louca, K. Watanabe, T. Taniguchi, A. I. Tartakovskii, G. Cerullo, and S. Dal Conte, Ultrafast exciton and trion dynamics in high-quality encapsulated mos2 monolayers, *physica status solidi (b)* **260**, 2200376 (2023).
- [48] T. Y. Jeong, S.-Y. Lee, S. Jung, and K. J. Yee, Photoinduced trion absorption in monolayer wse2, *Current Applied Physics* **20**, 272 (2020).
- [49] M. Selig, G. Berghäuser, M. Richter, R. Bratschitsch, A. Knorr, and E. Malic, Dark and bright exciton formation, thermalization, and photoluminescence in monolayer transition metal dichalcogenides, *2D Materials* **5**, 035017 (2018).
- [50] C. Pöllmann, P. Steinleitner, U. Leierseder, P. Nagler, G. Plechinger, M. Porer, R. Bratschitsch, C. Schüller, T. Korn, and R. Huber, Resonant internal quantum transitions and femtosecond radiative decay of excitons in monolayer wse2, *Nature materials* **14**, 889 (2015).
- [51] C. Robert, B. Han, P. Kapuscinski, A. Delhomme, C. Faugeras, T. Amand, M. R. Molas, M. Bartos, K. Watanabe, T. Taniguchi, B. Urbaszek, M. Potemski, and X. Marie, Measurement of the spin-forbidden dark excitons in mos2 and mose2 monolayers, *Nature Communications* **11**, 4037 (2020).
- [52] S. K. Pandey, R. Das, and P. Mahadevan, Layer-dependent electronic structure changes in transition metal dichalcogenides: The microscopic origin, *ACS Omega* **5**, 15169 (2020).
- [53] G. Christmann, R. Butté, E. Feltn, A. Mouti, P. A. Stadelmann, A. Castiglia, J.-F. Carlin, and N. Grandjean, Large vacuum rabi splitting in a multiple quantum well gan-based microcavity in the strong-coupling regime, *Physical Review B* **77**, 085310 (2008).
- [54] A. V. Zasedatelev, A. V. Baranikov, D. Sannikov, D. Urbonas, F. Scafrimuto, V. Y. Shishkov, E. S. Andrianov, Y. E. Lozovik, U. Scherf, T. Stöferle, et al., Single-photon nonlinearity at room temperature, *Nature* **597**, 493 (2021).
- [55] B. Stern, X. Zhu, C. P. Chen, L. D. Tzuang, J. Cardenas, K. Bergman, and M. Lipson, On-chip mode-division multiplexing switch, *Optica* **2**, 530 (2015).
- [56] P. S. Chakraborty, A. S. Cardoso, B. R. Wier, A. P. Omprakash, J. D. Cressler, M. Kaynak, and B. Tillack, A 0.8 THz f_{MAX} Si Ge HBT operating at 4.3 K, *IEEE Electron Device Letters* **35**, 151 (2014).
- [57] X. Lin, Y. Rivenson, N. T. Yardimci, M. Veli, Y. Luo, M. Jarrahi, and A. Ozcan, All-optical machine learning using diffractive deep neural networks, *Science* **361**, 1004 (2018).
- [58] T. Wang, M. M. Sohoni, L. G. Wright, M. M. Stein, S.-Y. Ma, T. Onodera, M. G. Anderson, and P. L. McMahon, Image sensing with multilayer nonlinear optical neural networks, *Nature Photonics* **17**, 408

- (2023).
- [59] D. E. Chang, A. S. Sørensen, E. A. Demler, and M. D. Lukin, A single-photon transistor using nanoscale surface plasmons, *Nature Physics* **3**, 807 (2007).
 - [60] S. Sun, H. Kim, Z. Luo, G. S. Solomon, and E. Waks, A single-photon switch and transistor enabled by a solid-state quantum memory, *Science* **361**, 57 (2018).
 - [61] O. Del Pozo-Zamudio, A. Genco, S. Schwarz, F. Withers, P. Walker, T. Godde, R. Schofield, A. Rooney, E. Prestat, K. Watanabe, *et al.*, Electrically pumped wse₂-based light-emitting van der waals heterostructures embedded in monolithic dielectric microcavities, *2D Materials* **7**, 031006 (2020).
 - [62] E. Maggiolini, L. Polimeno, F. Todisco, A. Di Renzo, B. Han, M. De Giorgi, V. Ardizzone, C. Schneider, R. Mastroia, A. Cannavale, *et al.*, Strongly enhanced light–matter coupling of monolayer ws₂ from a bound state in the continuum, *Nature Materials* **22**, 964 (2023).
 - [63] T. Weber, L. Kühner, L. Sortino, A. Ben Mhenni, N. P. Wilson, J. Kühne, J. J. Finley, S. A. Maier, and A. Tittl, Intrinsic strong light-matter coupling with self-hybridized bound states in the continuum in van der waals metasurfaces, *Nature Materials* **22**, 970 (2023).
 - [64] M.-A. Miri and A. Alu, Exceptional points in optics and photonics, *Science* **363**, eaar7709 (2019).
 - [65] J. Doppler, A. A. Mailybaev, J. Böhm, U. Kuhl, A. Girschik, F. Libisch, T. J. Milburn, P. Rabl, N. Moiseyev, and S. Rotter, Dynamically encircling an exceptional point for asymmetric mode switching, *Nature* **537**, 76 (2016).
 - [66] A. Raja, L. Waldecker, J. Zipfel, Y. Cho, S. Brem, J. D. Ziegler, M. Kulig, T. Taniguchi, K. Watanabe, E. Malic, *et al.*, Dielectric disorder in two-dimensional materials, *Nature nanotechnology* **14**, 832 (2019).
 - [67] K. W. Song, S. Chiavazzo, and O. Kyriienko, Microscopic theory of nonlinear phase space filling in polaritonic lattices, *Physical Review Research* **6**, 023033 (2024).
 - [68] C. Robert, T. Amand, F. Cadiz, D. Lagarde, E. Courtade, M. Manca, T. Taniguchi, K. Watanabe, B. Urbaszek, and X. Marie, Fine structure and lifetime of dark excitons in transition metal dichalcogenide monolayers, *Phys. Rev. B* **96**, 155423 (2017).
 - [69] M. Selig, G. Berghäuser, A. Raja, P. Nagler, C. Schüller, T. F. Heinz, T. Korn, A. Chernikov, E. Malic, and A. Knorr, Excitonic linewidth and coherence lifetime in monolayer transition metal dichalcogenides, *Nature Communications* **7**, 13279 (2016).